JOURNAL OF PETROLOGY | VOLUME 39 | NUMBER 6 | PAGES 1147–1167 | 1998

Formation and Evolution of Granite Magmas During Crustal Reworking: the Significance of Diatexites

E. W. SAWYER*

SCIENCES DE LA TERRE, UNIVERSITÉ DU QUÉBEC À CHICOUTIMI, CHICOUTIMI, QUÉBEC G7H 2B1, CANADA

A continuous section through reworked Archaean crust records the generation of granitic magma and its subsequent development in the Opatica subprovince in the Canadian shield. There, the transition from palaeosome to granite was a closed-system process through intermediate stages of patch migmatite and diatexite. The average degree of partial melting was less than 30%, but the melt fraction was redistributed within individual diatexite layers during deformation. Regions that lost melt became residual diatexites enriched in TiO_2, FeO_T, MgO, CaO, Sc, Cr, Co, Sr, rare earth elements (REE) and high field strength elements (HSFE). Melt accumulated to create diatexite magmas enriched in large ion lithophile elements (LILE), but contaminated with residuum material. Such diatexite magmas are parental to granites found at higher crustal levels in the terrane. Flow of the diatexite magma in response to deformation separated some of its residuum into schlieren. Parautochthonous plutons were created where ascending granitic magma locally ponded below impermeable layers and structures. Magma left the anatectic region in dykes and lost its remaining residuum as it crystallized. Consequently, the allochthonous granite magmas that rose through 20 km of crust to feed the highest level plutons in this region are highly fractionated and essentially free of residuum.

KEY WORDS: *anatexis; diatexite; granite magma; melt; residuum*

INTRODUCTION

Partial melting in the lower to middle crust, and transfer of that melt to the upper crust, is believed to have caused the chemical differentiation of the continental crust (Lambert & Heier, 1968; Fyfe, 1973). Although the geochemical signature of crustal reworking is well known (Taylor & McLennan, 1985), the physical processes involved, particularly how granite magma is formed, remain controversial (Miller *et al.*, 1988; White & Chappell, 1990). A partially melted source can form a granitic magma only if large volumes of melt are separated from most of their residuum. Understanding this process is crucial to determining how crustal recycling and differentiation occurs. For example, melt–residuum separation could be a nearly perfect, single-stage process at the site of partial melting, as described for leucosomes in metatexite migmatites (Wickham, 1987*a*; Sawyer, 1991, 1994; Brown *et al.*, 1995). Alternatively, the separation could be an imperfect, multi-stage process that yields a magma with a large residual component, as is observed in diatexite migmatites (Bea, 1991; Greenfield *et al.*, 1996; Sawyer, 1996). The metatexite model necessarily produces leucocratic, residuum-free granites, such as those described by Le Fort (1981) and Montel *et al.* (1991), and maximizes the geochemical signature of crustal differentiation. In contrast, the diatexite model can produce residuum-rich granites, and so reduce the geochemical effect of crustal differentiation, as Chappell (1996) noted.

How anatectic magmas formed in the deeper crust evolve to the granitic magmas emplaced in the upper crust is also poorly known, because few crustal sections are continuous from partially melted source to upper-crustal magma sink (pluton). Instead, most crustal sections display either shallow level plutons or deeper anatectic rocks. Even if granite magmas have a residuum component near their source, this could separate as the magma rises to yield shallow level magmas that are residuum depleted (Miller *et al.*, 1992). Where and how this separation occurs is also poorly known.

The Opatica subprovince of the Superior Province contains reworked Archaean crust that displays a con-

*Telephone: 418 545 5011 5636. Fax: 418 545 5012.
e-mail: ewsawyer@uqac.uquebec.ca

tinuous section from mid-crustal anatectic rocks to shallow level granite plutons. Changes in texture, mineralogy and bulk geochemistry are used to examine two principal questions: (1) What is the nature of the protolith–migmatite–granite transition and the process that creates a granitic magma during anatexis? (2) What processes control the magma composition outside the source region?

GEOLOGICAL SETTING

The Opatica subprovince is a 200 km wide belt of amphibolite-facies plutonic gneisses, located in the southeastern part of the Superior Province (Fig. 1). It is bordered to the north by amphibolite- to granulite-facies metasedimentary rocks of the Quetico–Nemiscau subprovince, and to the south by low-grade rocks of the Abitibi subprovince. Based on structural relations (Sawyer & Benn, 1993) and Lithoprobe seismic reflection profiles (Calvert *et al.*, 1995), the Opatica is interpreted as the deeply eroded interior of an Archaean mountain chain, and the Abitibi as a shallow level section through its foreland fold and thrust belt. A shallow, (13°) north-dipping reflector, with south-verging structures in its hanging wall, is present in the crust below the Abitibi (Lacroix & Sawyer, 1995) and steepens to 30° as it extends more than 30 km into the mantle below the southern Opatica. This reflector is interpreted as the remains of a north-dipping Archaean subduction zone (Calvert *et al.*, 1995). The U–Pb ages of syntectonic monzodiorite plutons indicate that the main phase of collision occurred at 2696 ± 3 Ma (Davis *et al.*, 1995). High-grade metamorphism in the central Opatica subprovince post-dates the main phases (D_1 and D_2) of the collision, but is synchronous with the late stages of the D_2 deformation.

Structural mapping (Benn *et al.*, 1992; Sawyer & Benn, 1993) and Lithoprobe seismic reflection results from north of Matagami (Calvert *et al.*, 1995; Bellefleur *et al.*, 1998) indicate that the dextral strike-slip, Nottaway River Shear Zone is the only major fault to displace the migmatites (Fig. 1). The compositions of metamorphic minerals (e.g. Ti content of amphibole) change smoothly from south to north across the Opatica. Furthermore, temperature–time paths constructed from U–Pb dating of zircon, monazite and titanite (Davis *et al.*, 1995), and $^{40}Ar/^{39}Ar$ dating of hornblende and biotite indicate progressively later exhumation of the Opatica northwards from its southern edge to where the highest grade migmatites are located (Sawyer, in preparation). Thus, the Opatica appears to present a section of reworked Archaean crust without major tectonic disruption.

Most of the Opatica subprovince consists of a suite of grey gneisses that range in composition from quartz meladiorite through trondhjemite–tonalite to granodiorite. Leucocratic rocks predominate. U–Pb zircon crystallization ages of the grey gneisses range from 2761 to 2702 Ma (Davis *et al.*, 1995). Some of the grey gneisses partially melted to form a suite of migmatites, leucogranite plutons and dykes. The plutons and dykes occur throughout the Opatica, but the migmatites are restricted to its central part. Monazite and titanite from the anatectic rocks give U–Pb crystallization ages of 2678 ± 2 and 2676 ± 2 Ma, respectively (Davis *et al.*, 1995). The Nd–Sm isotopic compositions of anatectic rocks indicate that the pink granites were derived from the grey gneisses (Bédard & Ludden, 1997). Furthermore, Bédard & Ludden found no isotopic evidence for a young, mantle-derived, mafic magma component in the crustal melting that formed the leucogranites.

METAMORPHISM

Most of the mafic rocks of the Opatica contain hornblende + andesine, which, together with rarer garnet- or clinopyroxene-bearing assemblages, imply amphibolite-facies conditions of metamorphism. Orthopyroxene has not been observed. Retrograde greenschist-facies mineral assemblages are developed in some late shear zones. The Ti content of amphiboles coexisting with a Ti-saturating phase increases with temperature (Spear, 1981). Results from 27 Opatica rocks show that the Ti content, per 23 oxygens, of amphibole coexisting with titanite and/or ilmenite increases from <0·045 in greenschist-facies rocks in retrograde shear zones and the adjacent northern Abitibi subprovince to 0·045–0·085 for amphibolite-facies rocks outside the migmatite zone, to maximum values of 0·075–0·165 for rocks from the migmatite zone. Using the Spear (1981) calibration, these Ti contents suggest a maximum temperature of 760°C is recorded in the migmatite zone. The empirical calibration of Schumacher *et al.* (1989) yields a temperature of ~810°C.

The Kohn & Spear (1990) garnet–amphibole–plagioclase barometer yields a pressure of 6·3 ± 1 kbar for garnet cores with included amphibole and plagioclase grains in amphibolites from just south of the migmatite zone in the eastern Opatica. However, garnet rims combined with matrix grains of amphibole and plagioclase give pressures of 7·1 ± 1 kbar. The Schmidt (1992) Al-in-hornblende barometer has been used for rocks that contain the assemblage hornblende + biotite + plagioclase + K-feldspar + quartz + titanite + ilmenite + melt + fluid. Three diatexite migmatites north of Matagami yield pressure estimates of 5·2–6·2 kbar for rim compositions. This geobarometer yields pressures of 1·7–2·6 kbar for two samples from the Canet

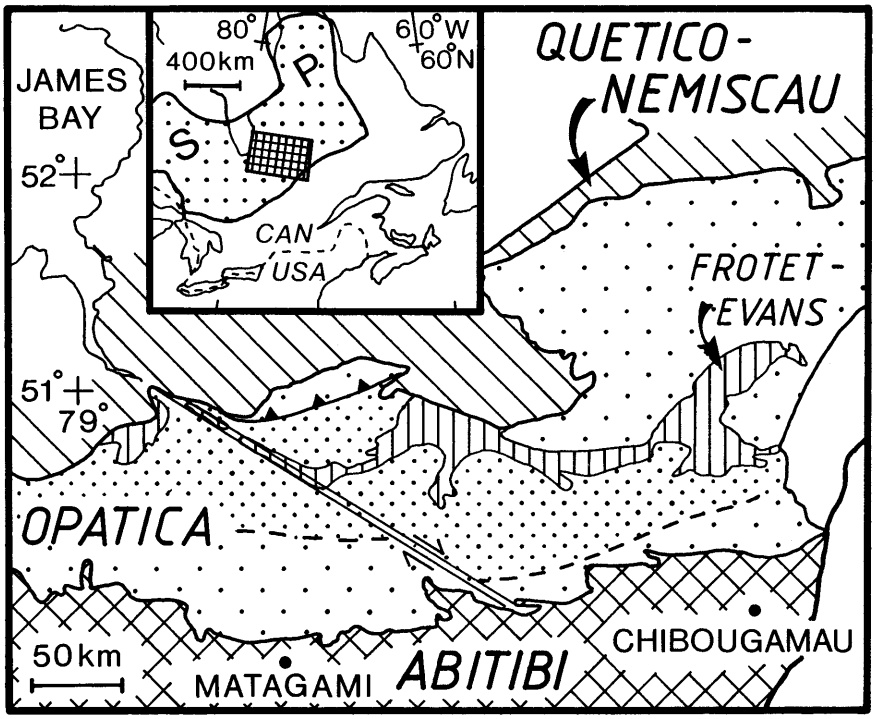

Fig. 1. Location of the Opatica subprovince in relation to the Abitibi and Quetico–Nemiscau subprovinces and the Frotet–Evans greenstone belt in the southeastern Superior Province (SP). The migmatite zone of the Opatica is shown in denser stipple and is crossed by the Nottaway River Shear Zone.

pluton, which intrudes the contact between the Opatica and Abitibi subprovinces.

MORPHOLOGY OF THE TRANSITION FROM GREY GNEISS TO GRANITE

Grey gneiss

Typical grey gneiss is a strongly foliated and/or banded leucocratic rock that contains scattered remnants of mafic material (Fig. 2a). The homogeneous and strongly penetrative nature of the S_1 foliation suggests that grey gneiss was deformed at high temperature in a crustal-scale shear zone (Sawyer & Benn, 1993). The microtexture formed during D_1 has been variably modified by dynamic recrystallization, and then by later grain growth during the 2678 Ma metamorphism. The typical grain size for felsic (>66% SiO_2) grey gneiss from the lower amphibolite facies is ~0·7 mm. Samples of grey gneiss that retain their S_1 foliation and banding in the migmatite zone represent bulk compositions too refractory to have become migmatized. However, the average grainsize of such rocks is increased to 1·4 mm.

The initial stages of migmatization

The first stage of migmatization produced small, widely scattered diffuse neosome patches (Fig. 2b) in which the S_1 foliation disappears and the grainsize has increased. This process only affected the leucocratic members of the grey gneiss that contain quartz, plagioclase and K-feldspar; hence, the term palaeosome applies only to these fertile bulk compositions. Other bulk compositions show no evidence for partial melting. Migmatites at this stage lack large changes of modal composition (Table 1), suggesting that the development of diffuse neosome patches was isochemical. As migmatization progressed the neosome patches enlarged and coalesced, leaving remnants of foliated grey gneiss in a coarser, homogeneous-textured neosome.

The first evidence for melt segregation (Fig. 2c) is the presence of small, medium-grained, pink leucosomes (e.g. sample EL268B) with diffuse borders in migmatites that display neosome patches. Typically, such leucosomes are in small shear zones and contain very little residuum material. Melt–residuum separation was evidently effective and probably driven by local shearing of the palaeosome. Evidence of melt segregation is seen in samples that contain coalesced patches. Two types of K-feldspar-depleted residual material formed at this stage: (1) darker patches, some of which show a remnant S_1 foliation,

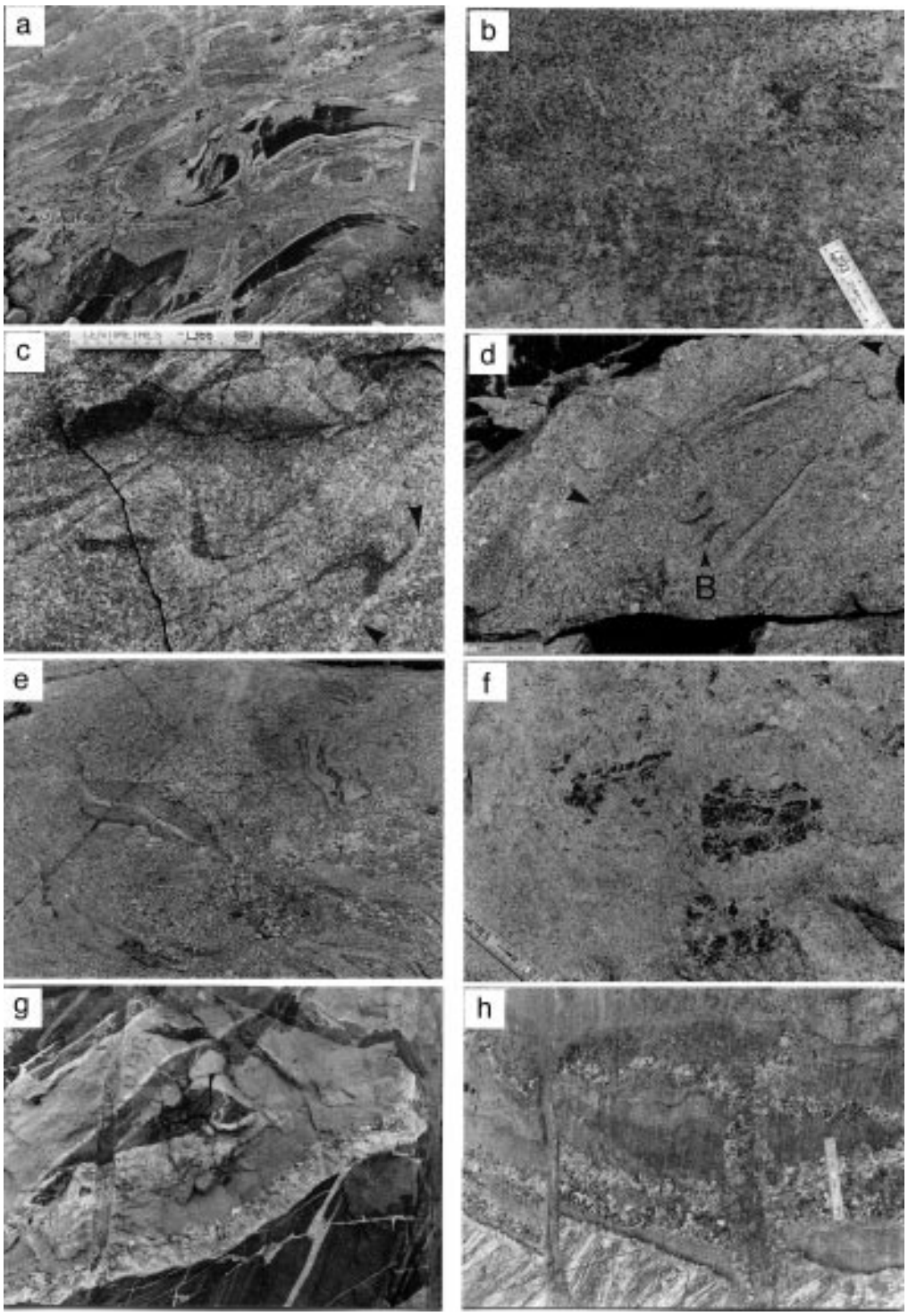

Fig. 2. (a) Typical non-migmatized grey gneisses containing disrupted mafic layers. (b) Beginning of migmatization, coarser-grained, neosome patches (upper left) within foliated palaeosome (near the scale). (c) The first segregation of melt forms small leucosomes (arrowed). (d) Grey diatexite containing flow banding marked by a layer richer in biotite (between arrows), incipient mafic schlieren (B) and the orientation of plagioclase-rich pods. (e) Pink diatexite with flow banding marked by schlieren and pods of residual diatexite. (f) Disaggregated mafic inclusions in a diatexite. (g) Leucogranite dykes in lower-amphibolite-facies rocks; the upper dyke has a narrow pink border and grey granodiorite interior, the lower consists of pink leucogranite and pegmatite. (h) Dykes feeding a high-level pluton with sub-horizontal layering. Scale is 15 cm long; in (e) the hammer head is 12 cm across, and in (g) field of view is 1·4 m wide.

Table 1: Average modal mineralogy and grain size of the principal rock types

	Quartz (%)	Plagioclase (%)	K-feldspar (%)	Biotite (%)	Opaques (%)	Assessories (%)	Grain size (mm)
Palaeosomes	29·9	56·6	8·4	4·8	0·2	0·1	1·34
range (n = 10)	21–38	47–67	2·5–13	1–7			
Patch migmatites	27·2	60·8	5·9	5·7	0·3	0·1	1·65
range (n = 4)	22–32	54–69	3–11	3–9			
Grey diatexites	29·6	55·5	10·2	4·4	0·2	0·1	1·69
range (n = 7)	23–31	47–60	5–17	2–7			
Pink diatexites	28·5	48·6	19·4	3·2	0·2	0·1	2·26
range (n = 9)	23–36	35–59	12–25	1–5			
Residual diatexites	24·8	63·6	0·3	10·4	0·6	0·3	
range (n = 8)	17–42	48–71	0–1·8	5–16			
Schlieren (n = 2)	17·9	58·5	0	22·5	0·5	0·6	
Parautochthonous granites	30·3	35·1	32·1	1·9	0·4	0·2	2·82
range (n = 11)	19–38	28–44	21–43	0·1–4·4			
Allochthonous granites*	30·6	37·7	29·7	1·8	0·2	trace	1·56
range (n = 8)	27–34	31–42	25–34	1–3·4			
Allochthonous granites†	30	33·2	35·4	1·2	0·2	trace	1·24
range (n = 9)	24–35	28–39	30–40	0·5–2·2			
Grey granodiorites	23·5	51·9	17·8	6·4	0·3	0·1	
range (n = 5)	22–25	48–58	8–22	2–11			

* Pink leucogranite dykes and sills intruded into migmatites.
†Pink leucogranite dykes and sills intruded into lower amphibolite facies rocks.
One thousand points per sample.

slightly richer in biotite, plagioclase and accessory minerals than the initial grey gneiss; and (2) light grey, leucocratic patches that consist principally of plagioclase, quartz and accessory minerals with minor biotite. These form from quartz-rich, leucocratic palaeosomes.

The diatexite

Textural homogenization affected larger volumes of rock as migmatization progressed. However, the most important development was that bulk flow occurred and produced dark- and light-coloured schlieren enriched in biotite and plagioclase, respectively (Fig. 2d). The schlieren define a flow-banding or layering. Locally there may also be asymmetrically shaped inclusions of (1) residual material, (2) palaeosome, (3) unmelted wall rock, and/or (4) plagioclase-rich pods (Fig. 2e) that possibly represent residuum or material crystallized from the melt. Such migmatites are confined between layers of less or unmigmatized grey gneiss. Rotation senses determined from the inclusion shape and irregularities in the flow-banding imply shear-driven flow of migmatite layers between the more competent grey gneiss walls. Because quartz grains in the diatexites are not greatly strained and igneous textures are preserved, flow probably took place in the partially melted state. The loss of pre-migmatization structures and the development of flow structures suggests that a larger melt fraction was present in these rocks compared with the patch migmatites. These migmatites (Fig. 2d and e) correspond to diatexite as described by Brown (1973, 1979), Sawyer & Barnes (1988), Bea (1991) and Sawyer (1996). Diatexite is the most abundant migmatite type in the Opatica subprovince and forms layers up to tens of metres thick. Some layers may be hundreds of metres thick, but there is insufficient continuous outcrop to be certain. Some diatexites contain coarse-grained leucocratic veins, or leucosomes (e.g. sample EL179), which post-date the flow-banding.

Diatexites show changes in colour, texture and composition linked to progressive migmatization (Table 1). Some are grey and display metamorphic textures (Fig. 3a). Some grey diatexites lack K-feldspar and have evidently lost their melt fraction; these are residual diatexites. Some residual diatexites form concordant layers tens of metres thick. More evolved diatexites are pink, and display greater K-feldspar contents, igneous-like textures

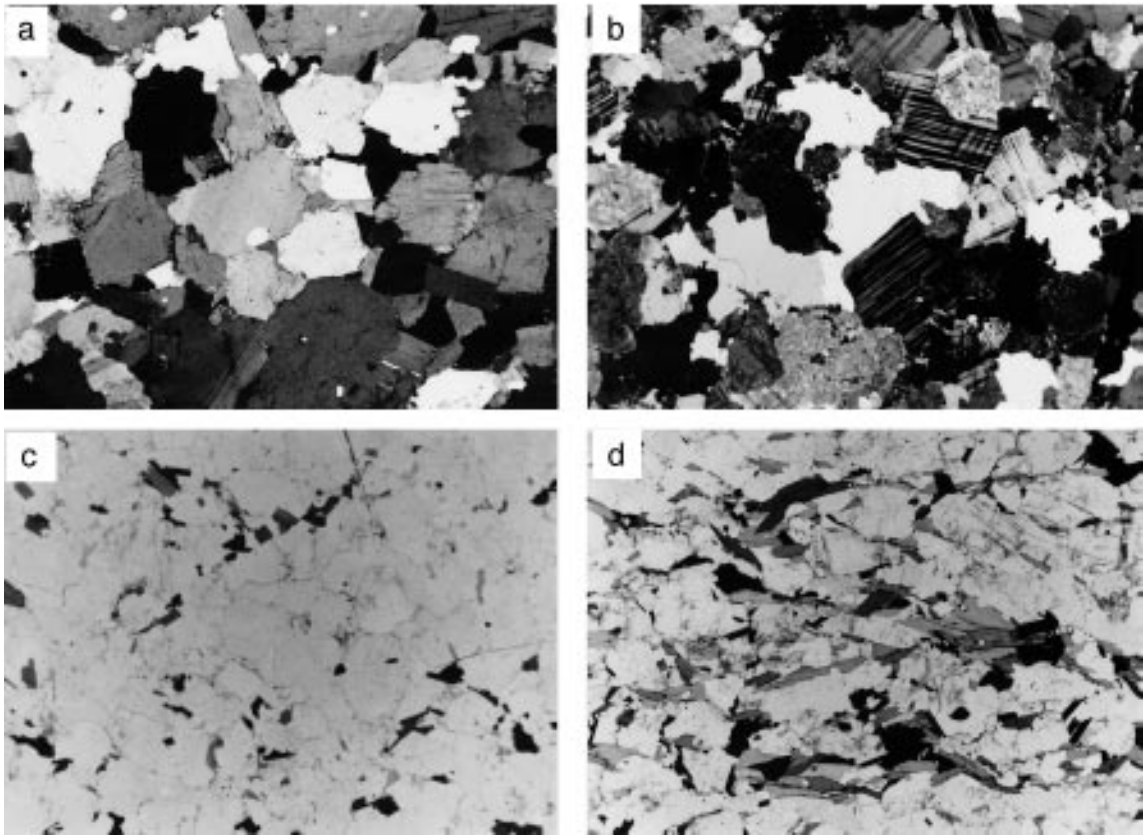

Fig. 3. Photomicrographs showing neosome textures. (a) Residual diatexite (note the large biotites and preponderance of equant plagioclase and quartz). (b) Pink diatexite, showing a large grain of quartz in the centre which has straight contact with microcline. (c) Distribution of biotite in a residual diatexite without a strong preferred orientation. (d) Distribution of biotite and prismatic plagioclase in a schlieren (note shape preferred orientation, perhaps indicative of tiling). (a) and (b) crossed polarizers; (c) and (d) plane-polarized light. Field of view is 7·5 mm, except for (a) where it is 6 mm.

(Fig. 3b), and a greater proportion of idioblastic–euhedral feldspar. The distribution of minerals is generally more uniform in the grey diatexite and residual diatexite (Fig. 3c) than in the pink diatexite, in which the biotite (and in some cases plagioclase) is concentrated into schlieren (Fig. 3d).

In places pink diatexite contains xenoliths derived from mafic dykes in the palaeosome. The xenoliths did not melt, but they did disaggregate and contaminate the diatexite with hornblende xenocrysts (Fig. 2f). Although this specific example is not petrologically significant as the diatexites do not generally contain hornblende, it illustrates a process of considerable importance in magma generation. As the diatexite flowed within the partially melted region it could have been contaminated with refractory or residual phases such as biotite, plagioclase and quartz, as the host rocks disaggregated.

The transition from patch migmatite to diatexite occurs on two scales. On the regional scale the transition occurs over hundreds of metres and is related to increase of metamorphic grade. On a local scale the transition occurs over a few metres and is related to variation in the fertility of the palaeosome.

The diatexite to granite transition

At the most advanced stage of migmatization large volumes of pink diatexite were able to move within the anatectic zone. Characteristically, such diatexites contain flow banding and schlieren. Diatexite is gradational, over distances of several to tens of metres, to granite in the field area, and locating the boundary between the two rock types is subjective. In this study, the term granite is used if the neosome texture is uniform (fewer schlieren and inclusions) over the scale of an outcrop. Small, biotite-rich folia are locally present in the leucogranite bodies. These folia are enriched in accessory phases; apatite, ilmenite, zircon, monazite, allanite and xenotime have been identified by electron microprobe.

Although there are no strictly *in situ*, or autochthonous, granite bodies in the Opatica, many granite bodies, some

several kilometres long, remain in the migmatite zone and are arguably parautochthonous. At their distal ends, bodies of the diatexite intrude across other units and contain country rock xenoliths; this suggests that they were magmas. Some granite magma has ponded beneath thick layers of unmelted (infertile) grey gneiss, or in gently dipping, north-vergent backthrusts (Fig. 4). At a smaller scale, the position and shape of the contacts of the parautochthonous granites is controlled either by fractures, or by minor folds formed during syn-anatexis, late D_2 deformation. Locally, at least, the granite contacts are discordant to S_1 in adjacent rocks. Contacts between parautochthonous granite bodies and competent wall rocks are sharp. However, where granite magma has intruded migmatitic wall rocks the wall rock structures are truncated (suggesting fracture), but the contacts are diffuse. This suggests that the partly melted wall rock and pluton magma interacted after fracture.

Granite outside the migmatite zone

Dykes and sills of anatectic granite occur throughout the Opatica subprovince. Those farthest from the migmatite zone intrude greenschist- to lower-amphibolite-facies rocks. All the intrusions have sharp, planar borders. Some contain fragments of wall rock; others display narrow, fine-grained margins. These features suggest fracture-controlled intrusion into cool rocks. Sharp-bordered dykes in the migmatite zone are late, and were evidently emplaced during the waning stages of anatexis.

There are two phases of allochthonous anatectic magma. One is a pink leucogranite, which ranges from fine-grained granite to coarse-grained pegmatite. Pegmatite is more abundant farther from the migmatite zone, a feature which may reflect increasing H_2O content of the magma as its crystallization progressed. The other anatectic granite type is a medium-grained, grey granodiorite to granite which locally contains wispy schlieren of biotite and nebulose patches of coarser-grained pink leucogranite. The grey phase is less common at the highest crustal levels (Fig. 4). Many dykes show characteristics intermediate between these two rock types, thus the relationship between the phases is ambiguous. Some zoned dykes (Fig. 2g) display a thin, pinkish (<1 cm), fine-grained outer zone, an intermediate zone of medium-grained, grey granodiorite and, in some cases an inner zone of coarse-grained pink leucogranite or pegmatite. Such relationships suggest that the two phases may reflect fractional crystallization of a common parent magma. However, elsewhere in the field area dykes and sills of the grey phase (with biotite schlieren and nebulose patches of pink granite) cut pink phase dykes and are themselves cut by still later pink phase dykes (Fig. 4). These features suggest that two magmas, which may, or may not, be genetically related, were present. The Nd–Sm isotopic compositions of the grey granodiorite (E.W. Sawyer, unpublished data, 1997) indicate that, like the pink granite, it was derived from the grey gneiss.

Although dykes and sills dominate, the Opatica subprovince also contains granite plutons. The deeper level plutons appear to consist of innumerable cross-cutting dykes of both the grey and pink granite phases. One such pluton, north of Matagami, has an exposed length of 300 m, and is located in the core of a regional-scale D_2 antiform mapped by Sawyer & Benn (1993). In contrast, the highest level plutons appear to be thin sheets that may be up to 20 km across [e.g. in domain 2 of traverse 2 mapped by Benn *et al.* (1992)]. One pluton, ~1 km across, located north of Chibougamau consists of subhorizontal sheets fed by pink leucogranite dykes (Fig. 2h). Each dyke appears to have introduced a small batch of magma into the pluton; pegmatite-textured dykes generate pegmatite-textured layers, and fine-grained dykes feed fine-grained layers. Successive feeder dykes cross-cut earlier batches of magma. Because several of the high-level plutons contain xenoliths of mafic volcanic rocks, they appear to have formed at the Opatica–Abitibi subprovince contact (Fig. 4). On the basis of geobarometry, this contact was a depth of 6–8 km when the plutons were intruded.

COMPOSITIONAL VARIATIONS OF PLAGIOCLASE AND BIOTITE

The field and petrographic relations indicate a transition from diatexite to granite by the separation of melt from residuum. In this section textural and compositional observations are used to distinguish which plagioclase and biotite grains in the neosomes are probably residual, and which crystallized from the melt. Major oxide abundances (>5%) were determined by energy dispersive, and minor oxides (e.g. TiO_2, MnO, CaO and Na_2O in biotite) were determined by wavelength dispersive electron microprobe analysis. Relative standard deviation for the major oxides is <1%, and <3% for TiO_2 at the concentrations found in the Opatica biotites.

Plagioclase grains from palaeosome samples show simple zoning patterns. Some of these rocks contain unzoned plagioclase, but generally the rims are more sodic than the cores. Typical compositions are An_{25} and An_{19}. Most plagioclase grains from the residual diatexite and schlieren samples are generally zoned. Some display rounded cores that are as calcic as An_{24}, with rims weakly zoned from An_{20} to $An_{17–18}$ at the outer edge. Two populations of plagioclase are present in the pink diatexite and parautochthonous granite samples. One has calcic cores of similar size and composition to those in residual diatexites, but with wider sodic rims zoned from An_{20} to

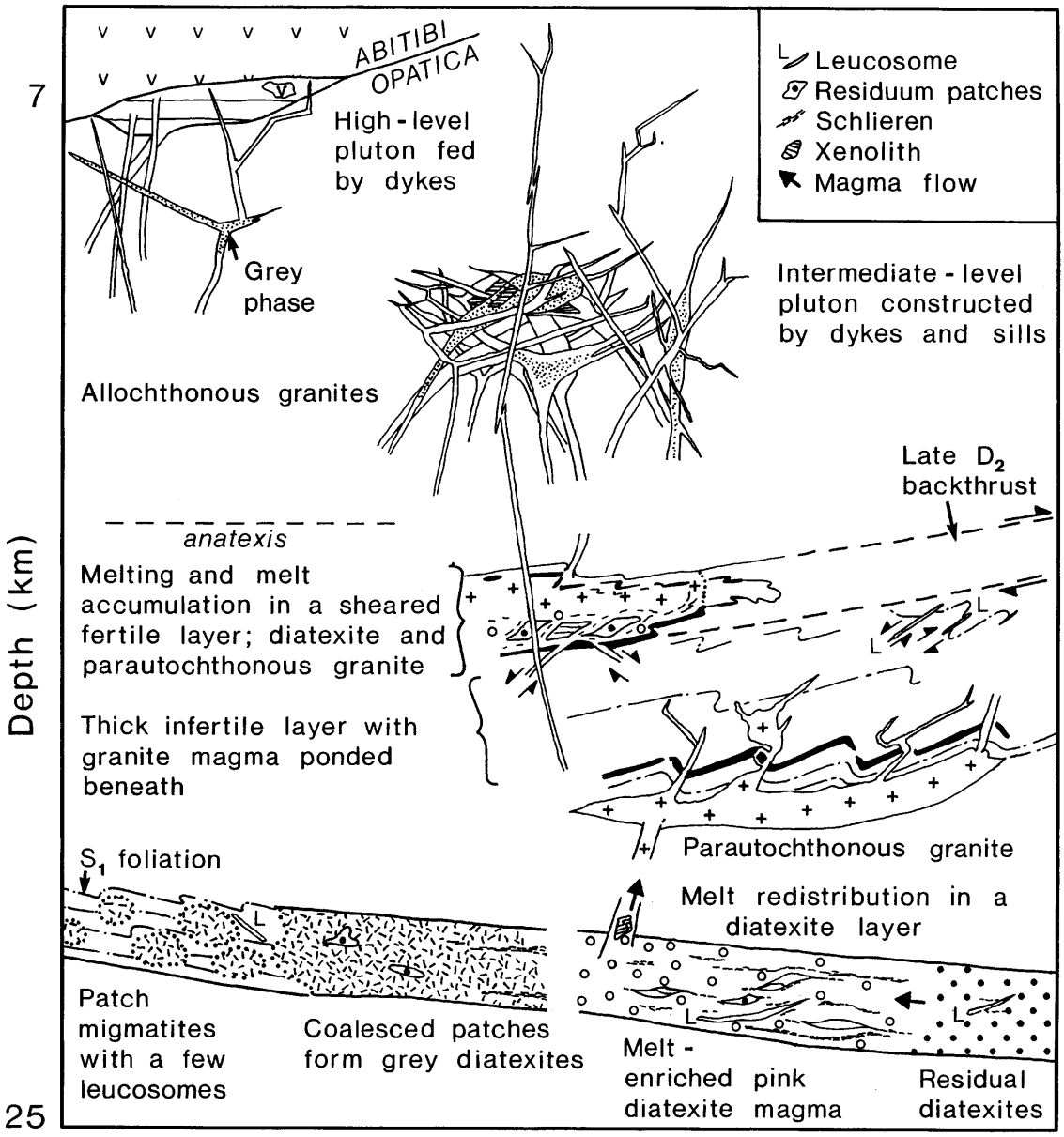

Fig. 4. Schematic representation (not to scale) of the field relations in the Opatica crust. Depths are approximate and based on geobarometry.

An_{16}. The second, more numerous, population lacks the calcic cores and is weakly zoned from An_{20-21} to An_{16-18} at the edge. Biotite inclusions are absent from the calcic cores, but present in some grain rims and in grains that lack calcic cores. The calcic cores are interpreted as residual (i.e. remnants from the palaeosome), and the more sodic plagioclase as crystallized from the anatectic melt.

Although biotite shows little variation in X_{Mg} within an individual sample, X_{Mg} increases by up to 0·04 in biotite grains adjacent to magnetite. The greatest compositional variation in the biotite is in its Ti content. The distribution of Ti content within the biotite population from residual diatexites (Fig. 5a and b) and schlieren (Fig. 5e and f) resembles the range found in biotite grains from the palaeosome. The highest Ti contents of biotite are found at the edges of large, slightly ragged grains associated with magnetite. Some residual rocks (Fig. 5b) and schlieren (Fig. 5f) contain a few small, isolated, elongate, low-Ti biotites located on grain boundaries.

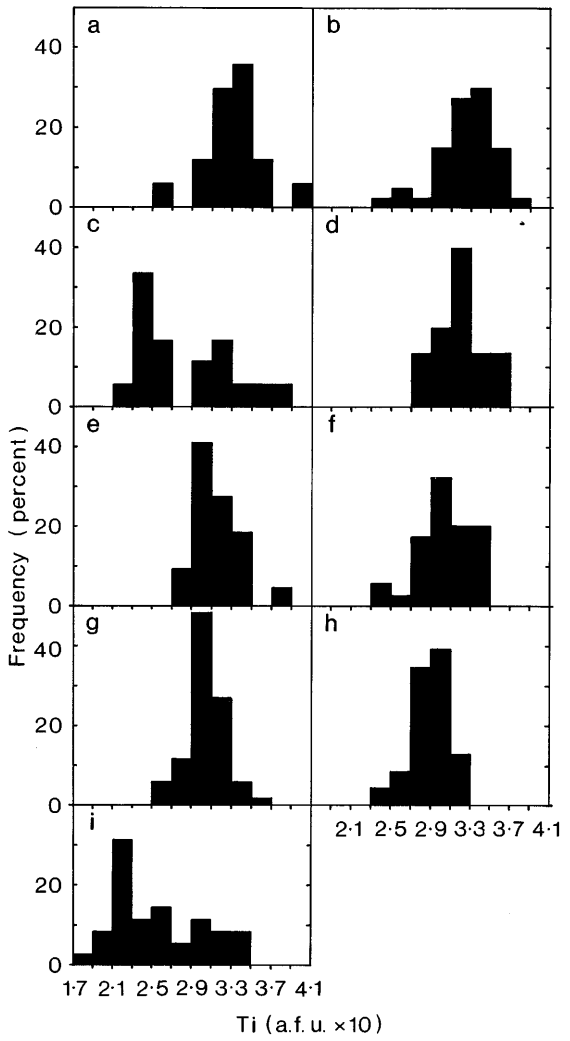

Fig. 5. Histograms for the Ti content, in atoms per 22 oxygen formula unit (a.f.u. × 10) of biotite from the anatectic rocks. (a) and (b) Residual diatexites, (c) and (d) their associated pink diatexites. (e) and (f) Biotite-rich schlieren, (g) and (h) their associated pink diatexites. (i) Grey granodiorite dyke. The width of each column is ~1·3 times the relative standard deviation of analysis.

Biotite populations in the pink diatexites are similar in composition to those (Fig. 5d, g and h) from the residual rocks and schlieren, suggesting that most of the biotite in the former is residual. However, some pink diatexites contain large numbers of low-Ti grains, which generate a bimodal distribution of composition (Fig. 5c). In all such rocks the low-Ti grains are isolated, small, elongate grains located along quartz and feldspar grain boundaries, whereas the more equant high-Ti grains are large and occur in clusters. The high-Ti biotite grains were probably inherited from the palaeosome, whereas the small, low-Ti biotite grains probably crystallized from the anatectic melt. The most titaniferous biotite grains in all samples form small, rounded inclusions in the outer parts of plagioclase grains, or rarely in interstitial quartz; these are probably relics of unstable residual biotite. Although the low-Ti grains may be numerous, they remain volumetrically minor, hence their X_{Mg} is buffered during retrograde cation exchange by the large reservoir of residual biotite.

Rocks derived from magmas that left the migmatite zone contain more complex biotite populations. A grey granodiorite (Fig. 5i) for example, contains: (1) large, high Ti-biotite grains probably derived from the residual rocks; (2) medium Ti-biotite grains (0·26 a.f.u.) that correspond to the low-Ti biotites from the diatexites; and (3) small, bladed low-Ti biotite grains (0·22 a.f.u.) which grew from the melt during its ascent.

WHOLE-ROCK GEOCHEMISTRY OF THE GREY GNEISS TO GRANITE TRANSITION

Analytical method

Some 117 samples of grey gneiss, diatexite migmatite, residuum material and leucogranite have been analysed. Between 1·5 and 5 kg of each sample was crushed and split to 200–250 g, which were pulverized in an aluminium oxide ceramic mill. The major oxides, except Na_2O, were determined on fused glass discs and the trace elements Nb, Ni, Sr, V, Y and Zr on pressed powder pellets, using standard X-ray fluorescence (XRF) methods at McGill University. Instrumental neutron activation analysis at Chicoutimi was used to determine Ba, Ce, Co, Cr, Cs, Eu, Hf, La, Lu, Na_2O, Nd, Rb, Sc, Sm, Ta, Tb, Th, Yb and U, after irradiation in a SLOWPOKE II reactor at École Polytechnique, Montreal; Bédard & Barnes (1990) gave details of the analytical method and errors. Representative samples are given in Table 2; anhydrous values are used in the text and figures. The full set of analyses is available from the author on request.

Grey gneiss

Grey gneiss samples plot in the calc-alkaline fields on discriminant diagrams, such as Peacock's (1931) CaO and (Na_2O + K_2O) vs SiO_2 and Irvine & Baragar's (1971) FeO_T–MgO–(Na_2O + K_2O) plot. Mantle-normalized multi-element patterns for the grey gneiss samples (Fig. 6a) show negative Nb and Ta anomalies, which indicate a subduction-related origin (Saunders *et al.*, 1980). Both results are compatible with the structural context of the suite.

Table 2: Representative whole-rock analyses

	Grey gneisses			Palaeosomes			Patch migmatites			Grey diatexites			Pink diatexites			Residual diatexites		
	EL143	EL209	EL180	EL268	EL200	EL382	EL269	EL267D	EL169	EL171	EL264B	EL334	EL197	EL360	EL356A	EL269A	EL267A	EL210
wt %																		
SiO_2	49·30	59·03	67·69	70·89	71·32	71·69	72·38	72·69	73·29	69·58	70·20	72·60	70·04	71·22	71·50	68·11	72·23	73·88
TiO_2	0·84	0·97	0·26	0·30	0·25	0·25	0·25	0·24	0·18	0·37	0·15	0·16	0·17	0·15	0·17	0·46	0·27	0·44
Al_2O_3	16·46	16·21	17·72	15·97	15·67	15·26	14·89	14·59	14·27	15·58	16·13	15·42	15·93	16·18	15·85	16·72	14·88	12·53
FeO_T	9·41	8·71	1·66	1·93	1·84	1·71	1·38	1·80	1·56	2·22	1·88	1·17	1·75	0·96	0·83	2·64	2·03	3·49
MnO	0·16	0·18	0·02	0·03	0·04	0·01	0·02	0·02	0·02	0·05	0·03	0·02	0·03	0·02	0·01	0·04	0·03	0·06
MgO	7·71	1·96	0·94	0·66	0·57	0·44	0·37	0·48	0·44	0·76	0·39	0·26	0·32	0·36	0·41	0·84	0·43	0·45
CaO	10·81	5·74	4·52	2·82	2·75	2·37	2·28	2·30	2·15	2·84	2·25	2·16	2·26	1·77	1·92	2·84	2·31	2·84
Na_2O	3·45	4·53	5·65	6·37	5·84	5·01	5·58	5·71	5·64	6·10	5·47	5·00	5·08	4·79	4·51	6·61	5·93	4·17
K_2O	0·80	1·51	1·00	1·10	1·41	2·35	2·03	1·45	1·03	1·90	2·37	2·47	3·19	3·57	3·76	1·07	1·36	0·90
P_2O_5	0·15	0·28	0·06	0·09	0·07	0·08	0·06	0·05	0·03	0·09	0·06	0·06	0·06	0·06	0·05	0·13	0·07	0·09
LOI	0·57	0·58	0·35	0·23	0·37	0·32	0·42	0·46	0·56	0·55	0·51	0·32	0·53	0·54	0·58	0·41	0·62	0·32
Total	99·66	99·70	99·87	100·39	100·13	99·49	99·66	99·79	99·17	100·04	99·44	99·64	99·36	99·62	99·59	99·87	100·16	99·17
ppm																		
Cr	268	8	8	7	4	6	4	2	3	12	7	<2	3	4	<2	6	<2	4
Ni	98	16	13	14	<10	n.d.	n.d.	<10	<10	<10	<10	<10	<10	<10	<10	<10	n.d.	20
Co	39	16	5	3	4	4	2	2	2	4	3	2	2	3	2	4	2	4
Sc	32·4	17·6	1·3	1·4	2·6	2·2	4·4	1·2	1·7	6·0	3·6	2·2	3·5	0·7	0·7	1·2	1·3	4·3
V	173	94	32	41	31	34	12	17	14	28	9	15	15	22	33	25	27	23
Rb	13	56	58	69	67	78	79	74	56	83	103	61	114	98	110	73	76	42
Cs	0·7	4·2	2·2	0·7	4·1	2·1	0·5	0·6	0·5	0·6	1·9	2·2	2·5	1·3	1·4	1·5	0·6	3·5
Ba	130	319	278	134	261	827	408	289	148	302	369	629	485	1347	1379	76	351	480
Sr	189	237	547	441	318	442	421	401	444	457	225	282	217	624	651	477	413	158
Ta	0·3	0·6	<0·2	1·2	0·7	0·5	1·4	0·5	0·4	2·2	1·0	<0·2	0·8	0·4	0·6	2·0	0·7	1·5
Nb	5	11	<2	12	6	7	16	5	7	22	15	4	11	2	5	31	8	9
Hf	1·7	5·0	2·5	4·1	3·2	3·3	2·9	3·7	3·1	4·5	4·6	2·6	3·8	2·8	3·5	4·8	4·7	8·3
Zr	65	192	75	139	122	123	96	113	100	154	115	94	99	90	116	171	140	287
Y	17	31	<2	10	10	3	16	6	3	18	80	5	63	<2	4	20	8	17
Th	0·7	1·6	<0·4	7·1	5·7	3·4	6·0	5·6	1·6	20·7	22·3	4·0	23·4	13·4	2·4	8·7	7·4	3·2
U	<0·4	0·6	<0·4	0·5	2·3	0·6	0·6	0·5	0·4	1·4	3·2	0·7	3·4	0·6	1·0	0·8	0·9	1·1
La	7·50	27·10	1·39	42·07	20·62	23·30	33·52	30·73	8·64	24·94	34·37	13·14	35·89	40·38	5·30	49·20	39·17	25·50
Ce	18·9	56·9	1·8	78·9	32·8	40·4	63·6	53·6	17·7	65·3	67·4	21·3	65·3	73·0	10·5	103·8	71·3	43·7
Nd	8·5	27·4	1·4	24·6	9·3	12·5	28·4	15·6	6·5	33·5	18·1	7·4	28·1	22·9	7·1	36·2	26·3	16·0
Sm	2·63	6·00	0·31	4·10	2·08	1·93	4·29	2·41	1·00	5·85	6·61	1·43	6·36	2·74	1·27	7·76	3·38	2·69
Eu	0·83	1·96	0·22	0·64	0·35	0·57	0·72	0·53	0·30	0·94	0·73	0·43	0·65	0·34	0·39	1·27	0·73	1·82
Tb	0·48	0·92	0·04	0·36	0·27	0·21	0·44	0·14	0·22	0·56	1·89	0·19	1·76	0·18	0·24	0·68	0·21	0·51
Yb	1·59	2·44	0·08	0·77	0·56	0·15	1·19	0·52	0·29	1·65	8·09	0·30	6·68	0·35	0·45	2·01	0·70	1·34
Lu	0·24	0·43	0·02	0·11	0·09	0·04	0·17	0·06	0·06	0·24	1·32	0·05	1·05	0·04	0·07	0·29	0·11	0·23

	Leucosomes		Parautochthonous granites			Allochthonous leucogranites				Grey granodiorites			Schlieren		
	EL268B	EL179	EL265	EL176	EL266	EL152	EL406	EL398	EL409	EL89	EL379	EL59	EL264A	EL356C	EL341
wt %															
SiO_2	73·82	74·74	66·67	69·30	73·25	72·42	74·52	75·67	73·64	63·12	69·29	73·37	61·59	66·72	75·72
TiO_2	0·18	0·08	0·56	0·28	0·21	0·17	0·08	0·02	0·01	0·79	0·25	0·13	0·59	0·32	0·25
Al_2O_3	14·24	13·44	15·30	16·31	12·87	14·17	14·09	13·56	14·25	17·53	16·32	14·58	16·90	18·59	13·15
FeO_T	1·13	0·85	3·58	2·00	1·93	1·82	0·75	0·48	0·31	3·91	1·60	1·03	7·53	1·84	1·97
MnO	0·02	0·01	0·07	0·04	0·02	0·03	0·02	<0·01	0·01	0·05	0·02	0·04	0·11	0·03	0·05
MgO	0·16	0·23	0·79	0·76	0·18	0·29	0·07	<0·01	0·05	1·56	0·36	0·20	1·57	0·94	0·63
CaO	1·65	0·75	1·75	3·52	0·70	1·63	1·00	1·11	0·17	3·67	2·41	1·59	2·58	3·25	1·77
Na_2O	4·81	3·47	4·92	6·24	3·49	3·47	3·12	3·47	2·94	5·79	6·03	4·62	5·40	7·31	4·25
K_2O	3·45	5·77	5·07	1·04	6·00	4·99	6·04	5·23	7·51	2·15	2·74	3·42	2·10	0·99	1·72
P_2O_5	0·02	0·02	0·30	0·08	0·07	0·05	0·02	0·02	0·03	0·28	0·10	0·03	0·24	0·10	0·02
LOI	0·28	0·47	0·67	0·73	0·74	0·50	0·41	0·28	0·35	0·61	0·29	0·40	0·77	0·65	0·50
Total	99·76	99·83	99·68	100·30	99·46	99·54	100·12	99·82	99·27	99·46	99·41	99·41	99·38	100·74	100·03
ppm															
Cr	5	<2	5	4	<2	<2	<2	<2	2	9	4	2	20	9	<2
Ni	<10	<10	<10	<10	<10	<10	<10	<10	<10	<10	80	n.d.	<10	<10	<10
Co	1	<2	5	4	<2	2	<2	<2	<2	8	3	2	9	5	3
Sc	0·6	2·6	3·4	6·4	3·4	3·2	1·3	1·3	3·5	4·6	1·6	2·1	13·1	1·5	4·2
V	21	14	48	21	20	17	<10	15	<10	64	17	12	51	18	31
Rb	123	164	245	23	265	147	178	161	186	116	119	117	224	76	55
Cs	0·5	1·0	3·0	<0·2	1·8	2·6	2·0	2·3	<0·5	5·1	3·2	14·7	8·1	2·2	4·2
Ba	888	456	996	147	324	1075	536	713	102	1050	1248	915	89	113	271
Sr	406	118	338	454	93	240	167	295	39	1206	851	308	202	736	224
Ta	0·9	<0·2	1·2	0·9	1·4	0·4	4·9	2·3	<0·2	1·9	0·4	0·8	1·5	0·9	2·3
Nb	8	3	18	16	14	5	24	13	4	13	4	7	53	9	23
Hf	2·3	3·2	8·9	4·0	5·1	6·2	2·9	3·0	1·3	5·4	3·1	2·3	15·7	4·0	0·9
Zr	79	80	341	143	160	169	67	52	20	259	131	76	508	137	17
Y	10	5	18	11	14	13	23	8	16	13	3	6	71	9	6
Th	4·9	18·9	22·4	15·4	55·9	49·9	13·7	10·1	2·3	8·9	5·0	3·9	52·0	3·1	1·4
U	0·6	4·2	3·8	0·8	5·4	9·5	11·8	9·6	0·4	2·2	1·3	1·1	4·5	0·8	0·6
La	22·40	20·99	102·40	22·79	70·81	63·18	7·10	3·90	6·62	59·00	26·00	9·30	88·89	7·69	3·66
Ce	46·3	42·7	194·1	56·0	129·2	110·8	16·5	7·2	8·5	103·6	54·4	16·0	170·7	17·0	6·3
Nd	21·4	13·0	72·5	22·3	46·5	31·2	<10·0	1·9	<10·0	39·4	16·1	5·9	53·3	7·5	1·4
Sm	3·88	3·70	11·64	4·48	7·10	7·05	2·60	0·55	0·40	5·85	3·22	1·17	15·39	2·87	0·49
Eu	0·62	0·28	2·08	0·97	0·57	0·89	0·38	0·20	0·12	1·55	1·02	0·34	0·72	0·61	0·30
Tb	0·37	0·33	0·82	0·50	0·56	0·69	0·57	0·20	0·14	0·45	0·22	0·11	2·46	0·38	0·13
Yb	0·82	0·32	1·42	1·32	1·42	1·14	1·87	2·22	1·48	0·77	0·22	0·35	6·24	0·92	0·71
Lu	0·10	0·05	0·24	0·17	0·24	0·19	0·32	0·43	0·25	0·11	0·05	0·04	1·04	0·13	0·13

n.d., not determined.

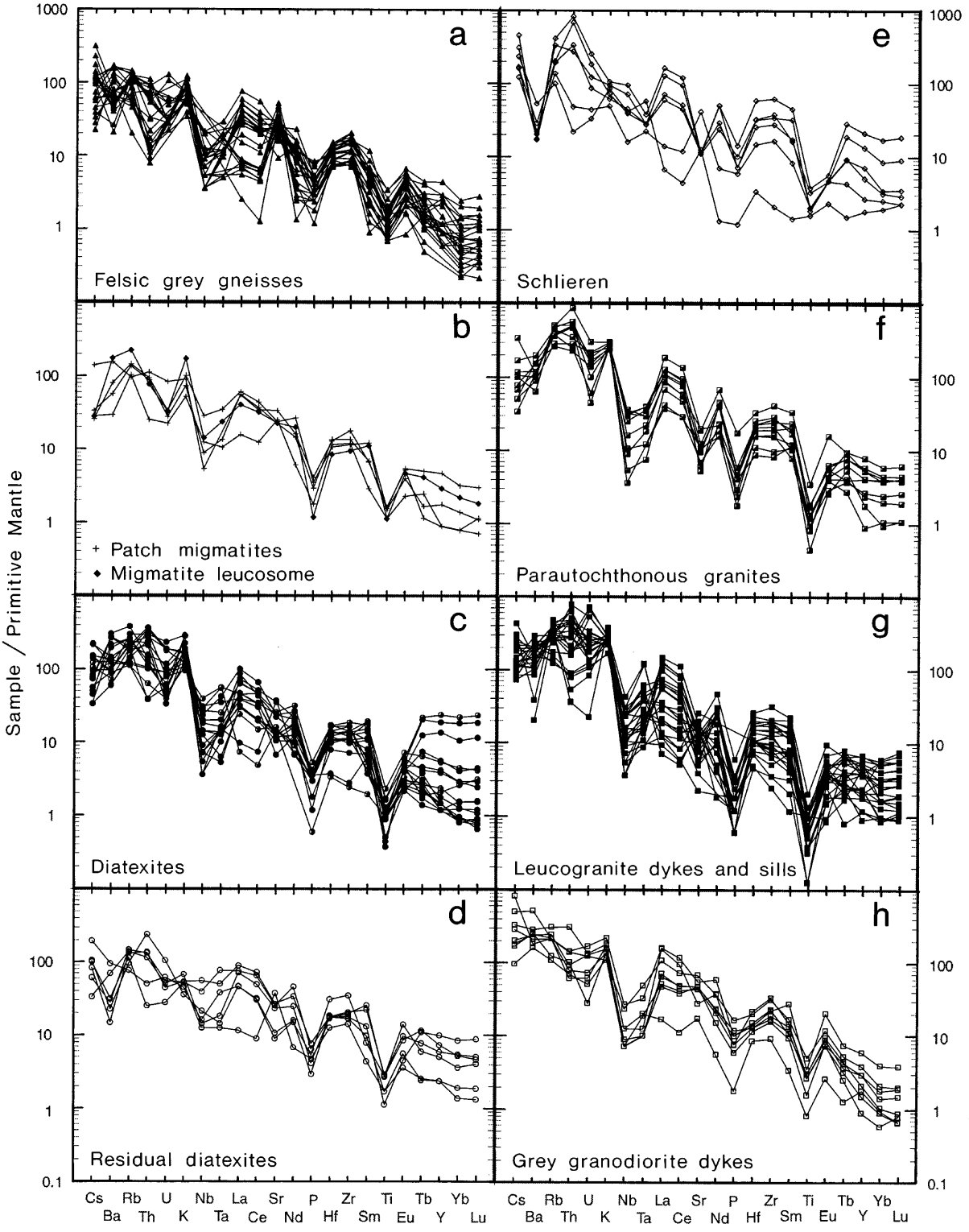

Fig. 6. Multi-element variation diagrams for the palaeosome–migmatite–granite transition, normalized to the primitive mantle of Taylor & McLennan (1985).

Felsic grey gneiss samples display negative P_2O_5 and TiO_2 anomalies, indicating the effects of prior crystallization of apatite and a Ti-bearing phase on the later, evolved magmas of the suite (Fig. 6a). About half of the felsic samples have prominent, positive Sr and Eu anomalies attributed to the accumulation of plagioclase. The largest anomalies occur in sample EL180, which has the lowest total rare earth element (REE) content and the highest plagioclase content (70·4%) of any felsic grey gneiss. Three samples have large negative Eu anomalies, which may indicate that they formed from magmas that had already crystallized substantial amounts of plagioclase; these samples also have the highest heavy REE (HREE) contents. Fractionation within the REE changes the average La/Yb_N ratio from mafic (2·6) through intermediate (9·3) to felsic (34·6) bulk compositions as HREE and Y contents decrease.

Harker diagrams for (FeO_T + MgO) (Fig. 7a), Sc, Ni and Co show steeper trends for samples with <68% SiO_2. This coincides with petrographic observations that hornblende disappears from rocks with greater than ~69% SiO_2, leaving biotite as the ferromagnesian phase. The K_2O (Fig. 7b), Rb, Sr, Ba, Cs and Na_2O contents all increase, but CaO (Fig. 7c) decreases with increasing silica content. The K_2O content increases with silica, but above 69% SiO_2 a steeper positive correlation reflects increasing modal K-feldspar. High SiO_2 samples with low K_2O contents represent plagioclase accumulations. Thus, the main compositional variations in the grey gneisses are consistent with fractional crystallization of hornblende, plagioclase and biotite.

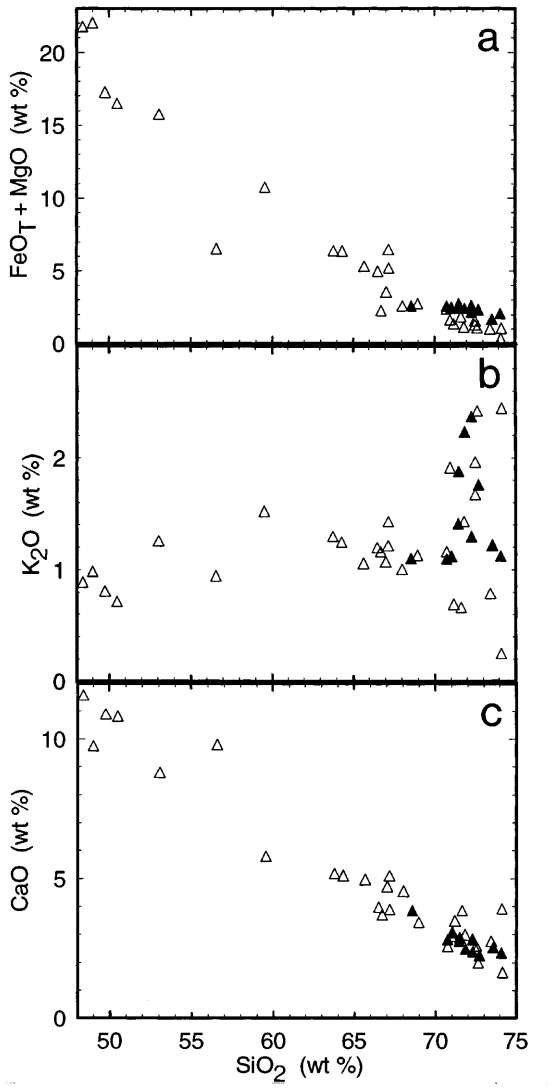

Fig. 7. Harker variation diagrams for the grey gneisses; filled symbols represent probable palaeosomes. (a) (FeO_T + MgO) and (b) K_2O show a change of slope for the high-silica samples. (c) CaO shows a linear trend with SiO_2.

Continuity from palaeosome to neosome

Although the neosomes inherited the negative Nb, Ta, P_2O_5 and TiO_2 anomalies of the grey gneiss (Fig. 6), not all members of the grey gneiss suite melted. Neither the patch migmatites nor the diatexites have the strong positive Sr or Eu anomalies shown by half of the grey gneiss samples. This feature, plus the absence of hornblende from the neosomes, constrains the palaeosomes to be the felsic grey gneiss with SiO_2 >69%, i.e. rocks that represent either primary melt, or fractionated melt compositions and with high HREE contents. The grey gneiss samples that show evidence for plagioclase accumulation were infertile and could not, therefore, represent palaeosomes (Fig. 7).

Patch migmatite samples have normalized multi-element patterns with similar shapes and slopes to the grey gneiss samples (Fig. 6a and b). In contrast, diatexite samples display a progressive enrichment in Ba, Rb, Th, U and K_2O with increased migmatization. These effects produce a hump shape at the left end of the pattern; some samples are HREE enriched (Fig. 6a–c). Residual diatexite samples (Fig. 6d) have flatter and smoother patterns than the palaeosome, patch migmatite or diatexite samples, because of their lower Cs, Ba, Rb and K_2O, but higher Y and HREE contents. Schlieren samples (Fig. 6e) show greater variability because some are plagioclase rich and others biotite rich; nevertheless, both types are rich in Cs, Rb, Th, U, Hf, Zr and REE.

All samples of leucogranite neosomes (Fig. 6f and g) have steeper patterns than the palaeosome, patch migmatite and diatexite samples, principally because of their high Rb, Th, U and K_2O contents. Some leucogranite dyke samples are strongly depleted in light REE (LREE) and this can produce positive Sr and Nb–Ta

anomalies (Fig. 6g). Grey granodiorite samples (Fig. 6h) have lower Th, U and K_2O, but higher Cs and Ba contents than associated leucogranite dyke rocks, and these effects eliminate the humped-shaped part of the pattern that is seen in other neosome samples (Fig. 6f and g). Grey granodiorite samples have the highest average La/Yb_N (55·2) of any neosome type.

Figure 6 shows evidence for a geochemical continuity not only across the palaeosome to granite transition, but also to the granites at higher crustal levels. Different factors can control composition at various stages through the transition. The three most important of these—source rock composition, melt–residuum separation and fractional crystallization—are considered next.

Palaeosome influence on diatexite composition

The effect that the palaeosome has on the composition of individual diatexites is best illustrated with samples from the same large (20–50 m across) outcrops. For example, at locality 293 (Fig. 8a) a flat HREE pattern with negative Sr and Eu anomalies of the palaeosome is found in all the diatexite samples, in the mafic schlieren they contain, and in a small parautochthonous granite. At outcrop 300 (Fig. 8b), small positive Sr and Eu anomalies and a distinctive enriched HREE pattern found in the palaeosome is carried through to the diatexite, the schlieren in it, and to a leucogranite vein. The HREE- and U-depleted patterns and weak Sr anomaly of the palaeosome at locality 259 (Fig. 8c) are also observed in samples of patch migmatite, diatexite, residua, and late fractionated diatexite leucosome. In another part of locality 259, a different palaeosome layer (Fig. 8d) with large negative Sr and Eu anomalies, and an HREE-depleted pattern is present. Its geochemical features are carried in samples of patch migmatite, fractionated diatexite leucosome and the residua derived from it. Because individual palaeosome characteristics appear in its neosomes, mixing of magma batches derived from different layers evidently did not occur at this stage of diatexite formation.

Melt–residuum separation and diatexite composition

The compositional field of the patch migmatite samples coincides with that of palaeosome samples (Fig. 9). This supports petrographic evidence that the onset of migmatization was essentially isochemical. However, the diatexite samples display a wider compositional range. Residual diatexite and schlieren samples are enriched in the compatible elements TiO_2, FeO_T, MgO, CaO, Na_2O and Cr relative to the palaeosome and grey diatexite

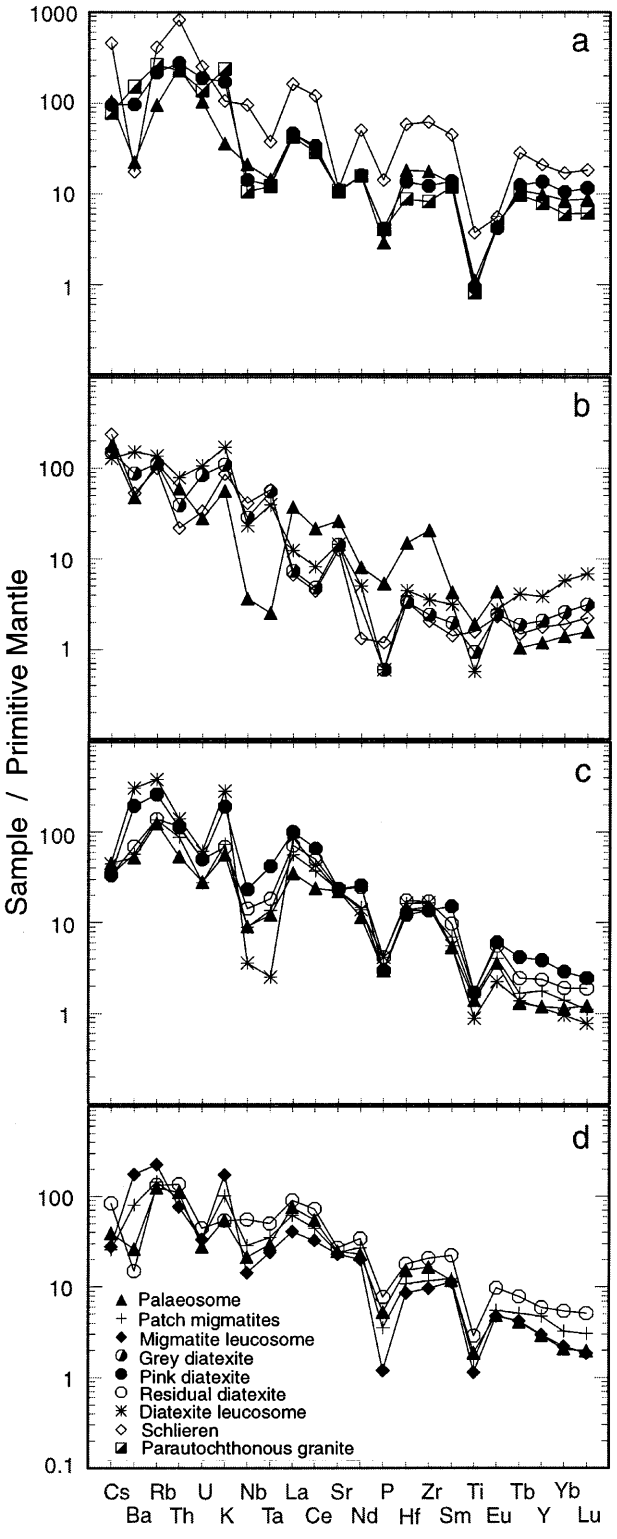

Fig. 8. Multi-element variation diagrams for individual outcrops, normalized to the primitive mantle of Taylor & McLennan (1985). The diagrams show that all the anatectic rocks of individual outcrops have the same general characteristics.

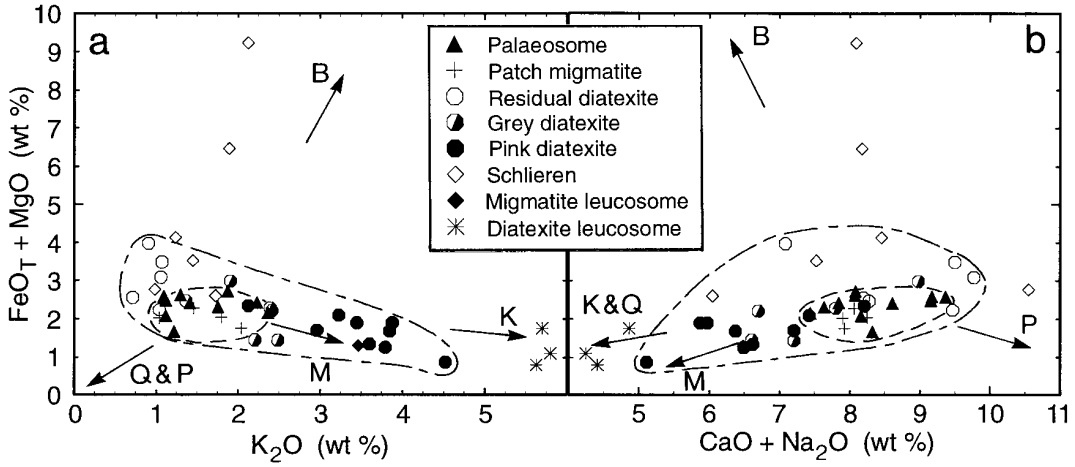

Fig. 9. Compositional trends in the diatexites; (a) (FeO_T + MgO) vs K_2O and (b) (FeO_T + MgO) vs (CaO + Na_2O). Position of the mineral vectors (B, biotite; K, K-feldspar; P, plagioclase; Q, quartz) is based on mineral compositions determined by electron microprobe; the melt vector (M) is based on the migmatite leucosome sample EL268B.

samples. In contrast, pink diatexite samples are enriched in the incompatible elements K_2O, Ba, Rb and SiO_2. The principal vectors that control diatexite composition are quartz, plagioclase, biotite, K-feldspar and melt (represented by the migmatite leucosome). Thus, Fig. 9 shows that pink diatexite samples are enriched in the melt component, whereas the residuum component is concentrated in the residual diatexite and the schlieren samples. Interestingly, some schlieren are enriched in biotite, others in plagioclase and still others in quartz. This reflects which phases were in excess during melting of a particular layer, and the different physical behaviour of the minerals during magma flow. The distribution of melt-rich and residuum-rich samples on opposite sides of the palaeosome field is consistent with closed-system migmatization, but the scale is much larger than for the patch migmatite case.

The trace elements Hf, Zr, La, Ce and Sm are enriched in the residual diatexites and schlieren relative to the palaeosome and the pink diatexites (Fig. 6). The distributions of Th, Y and HREE are enriched in all the residual diatexites, and in a few of the grey and pink diatexites, relative to the palaeosome. This supports the petrographic observation that the accessory phases containing the high field strength elements (HFSE) and REE are concentrated in the residuum and schlieren.

Granitic neosome compositions

Granitic neosome samples range from high-silica (72–76% SiO_2) pink leucogranite dykes to grey granodiorite dykes that contain 64–74% SiO_2. The range of overlap between the pink and grey phases coincides with values for melt-rich diatexite samples (Fig. 10). In all neosome groups TiO_2, Al_2O_3, FeO_T, MgO, CaO, P_2O_5, Cr, Sc, Co, V, LREE, Sr, Eu, Hf and Zr show negative correlations with SiO_2. Only K_2O and Rb show positive correlations with SiO_2 in neosome samples and were incompatible with the crystallized phases. Sample EL265, a parautochthonous granite that contains small mafic folia, plots out of the leucocratic granite field (Fig. 10) and illustrates the effect of entrained residuum material on neosome composition.

Grey granodiorite samples display the highest (FeO_T + MgO) and (CaO + Na_2O) abundances of the granitic neosomes, which reflects their higher biotite and plagioclase contents. These samples have higher and flatter trends for (CaO + Na_2O) and Al_2O_3 vs SiO_2 (e.g. Fig. 10c) than those samples with >72% SiO_2. In the absence of other major CaO- and Na_2O-bearing phases, such correlations indicate crystallization of progressively more sodic plagioclase as SiO_2 content of the magma rises. Figure 11 shows that the grey granodiorite samples and sample EL176 have lower Rb/Sr ratios (<0·38) than most of leucogranite samples (0·29–3·9). A region of overlap coincides with the field of melt-rich diatexite samples. The very high CaO, Na_2O and Sr contents of grey granodiorite samples suggests they probably accumulated early-crystallized plagioclase.

Granitic neosome samples that show positive Eu anomalies are uncommon (16% of samples) in the Opatica. As most (78%) diatexite samples have negative Eu anomalies the melts, or magmas, derived from them will also show negative Eu anomalies. Consequently, Eu concentration by plagioclase accumulation may not generate a rock with a positive Eu anomaly from an initial melt with a low Eu content. Samples that represent

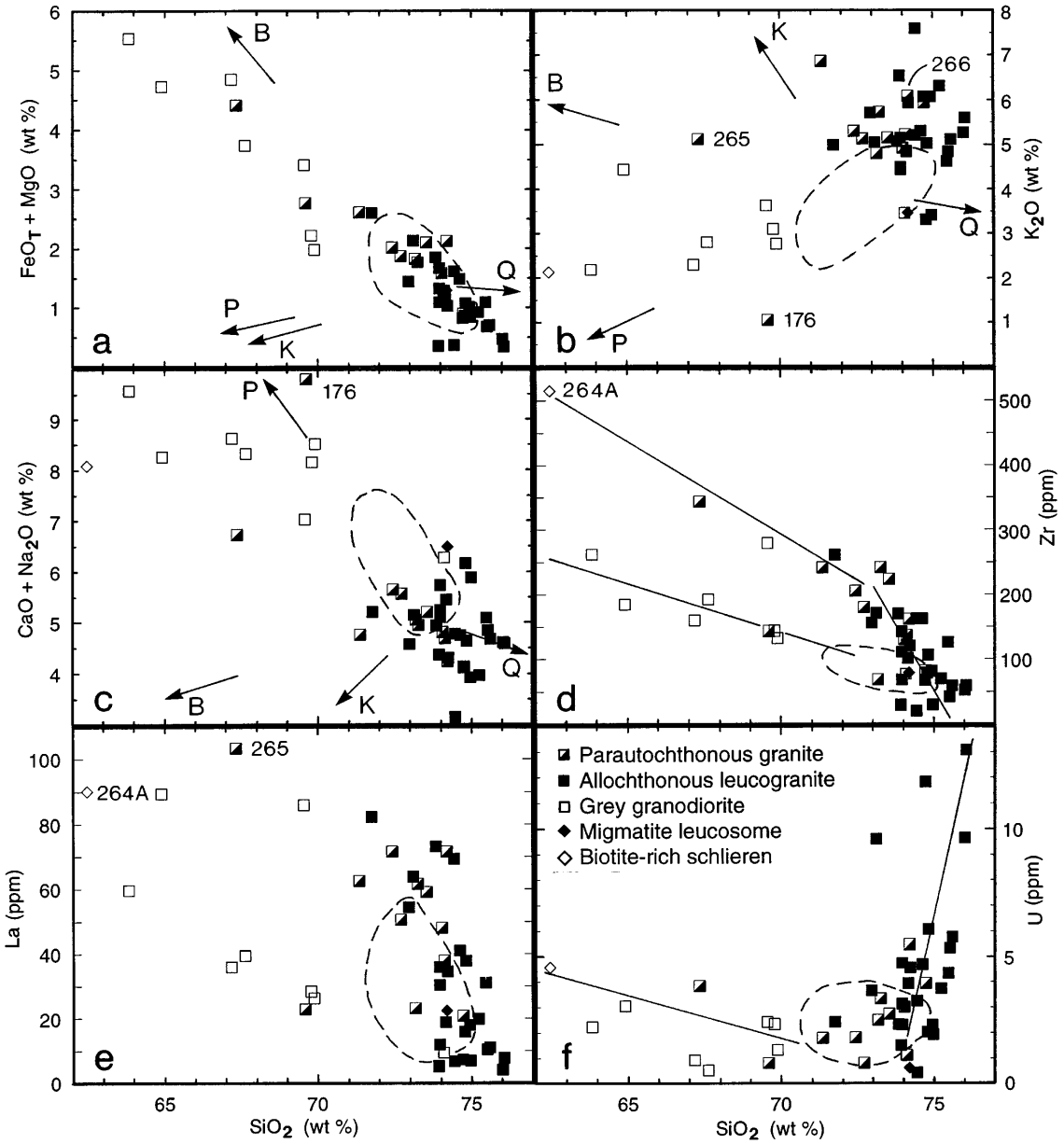

Fig. 10. Harker diagrams showing the compositional variation in the granitic neosomes; (a) (FeO_T + MgO), (b) K_2O, (c) (CaO + Na_2O), (d) Zr, (e) La and (f) U. Both Zr and La show two shallow, negative trends for the plagioclase-rich, low-silica samples, and a steeper negative trend in the high-silica samples as a result of fractionation of crystallized accessory phases. In contrast, U increases in the high-silica samples, suggesting incompatible behaviour. Dashed line marks the field of the melt-enriched (pink) diatexite source magma.

accumulations of plagioclase should, at least, have Eu anomalies that are less negative than the associated evolved melts. This is observed in granite samples from the migmatite zone (Fig. 12a and b). Outside the migmatite zone, some dykes of the grey granodiorite show positive Eu anomalies, whereas associated pink granite dykes all have negative Eu anomalies (Fig. 12c). As the SiO_2 and K_2O contents and Rb/Sr ratios of leucogranite samples increase, their total REE contents and La/Yb_N ratios also tend to increase. Towards the end of the crystallization sequence (SiO_2 >74%, K_2O >5·5%), white or texturally different (e.g. pegmatite EL398 and aplite EL409) varieties of the pink leucogranite develop. These rocks display lower total REE contents, and have V-shaped patterns because of LREE and middle REE depletion compared with other leucogranite samples

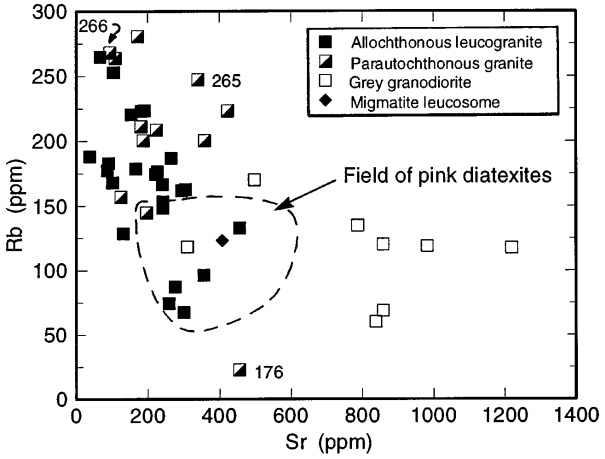

Fig. 11. Rb vs Sr plot for the parautochthonous and allochthonous granites.

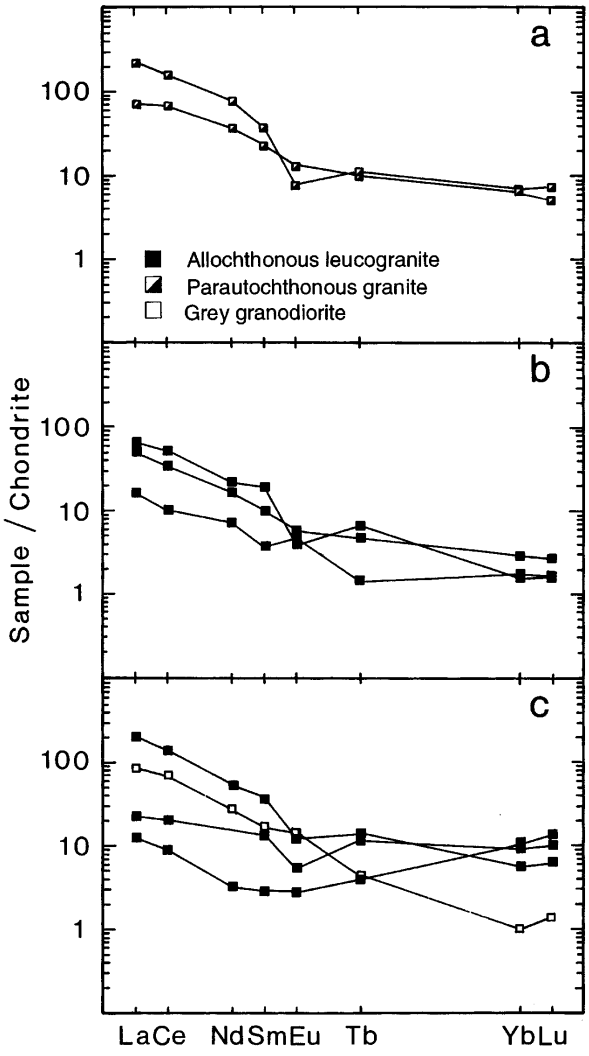

Fig. 12. Chondrite-normalized [values from Taylor & Gorton (1977)] rare earth patterns for parautochthonous granites (a) and allochthonous granite dykes; (b) from the migmatite zone; and (c) from outside the migmatite zone.

(Fig. 12c). Some of these highly fractionated samples also show depletion of Hf and Zr, in some cases along with a marked enrichment of Nb, Ta, Th and U.

For samples with >72% SiO_2 the trace elements Y, Yb, Lu, Nb, Ta and U all show strong positive correlations with SiO_2, i.e. incompatible behaviour (Fig. 10f). However, in the same samples La, Ce, Hf, Zr and, to a lesser extent, Th show strong negative correlations (Fig. 10e) implying the compatible behaviour that has been noted in other granitic magmas (e.g. Tindle *et al.*, 1988). In contrast, all these elements show much flatter negative correlations with SiO_2 for samples with <72% SiO_2. Such a complex trace element distribution probably reflects both crystallization and/or fractionation, and contamination by disaggregated residual material.

Zirconium can be used to examine these effects because its concentration in metaluminous–peraluminous melts can be estimated from the data of Watson & Harrison (1983). Approximately 125 ppm Zr is required to saturate the Opatica leucogranite melts at an assumed melting temperature of 760°C, and ~27 ppm at near-solidus temperatures of 650°C. Thus, most of the pink granite dykes (<150 ppm Zr), and the pegmatite, aplite and white dykes (<52 ppm Zr), probably crystallized from low-temperature melts saturated in Zr. However, one of the dykes and five of the parautochthonous granite samples contain between 200 and 341 ppm Zr, which implies (1) accumulation of magmatic zircon, (2) the presence of xenocrystic zircon, or (3) a far higher melting temperature for these samples. Because the zircons (Davis *et al.*, 1995) and monazites (L. P. Bédard, unpublished data, 1994) in leucogranite samples from the migmatite zone consist of inherited cores with only thin magmatic overgrowths, the second alternative is preferred. There are three trends on the Harker diagram for Zr (Fig. 10d). For samples with <72% SiO_2, the first (upper) trend includes five of the parautochthonous granite samples and one grey granodiorite. This trend projects from the parautochthonous granite through sample EL265 to the mafic schlieren (e.g. sample EL264A). It may, therefore, represent a mixing line between magma and zircon-bearing residuum. The second is a lower trend that extends from the field of melt-rich diatexite and includes most of the grey granodiorite samples and sample EL176. The lower trend appears to represent the magma plus residuum mixture diluted by the accumulation of plagioclase. The third trend is much steeper. It includes all samples with <160 ppm Zr and >72% SiO_2 and probably

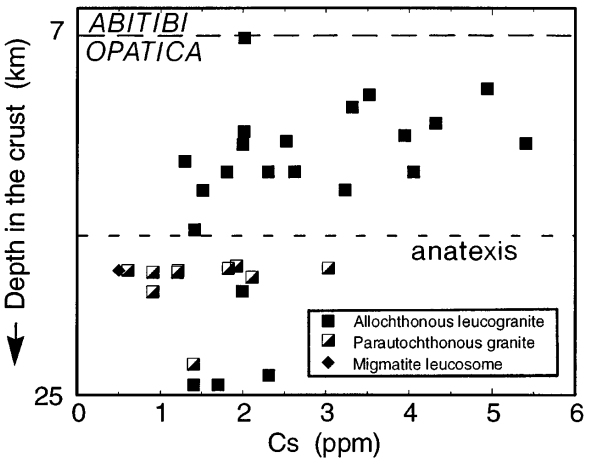

Fig. 13. Plot showing that the concentration of the incompatible element Cs increases in the pink leucogranite magma with crustal level. Depths are approximate and based on geobarometry.

reflects the effects of zircon fractionation. A similar pattern is shown by La, Ce and Th, which suggests additional controls by monazite and/or allanite, minerals already identified in, and likely to be concentrated in, the residuum (Fig. 10).

The range of neosome compositions from grey granodiorite to the pink leucogranite is consistent with both magmas having been derived from a common parent that resembled the melt-rich diatexites. Grey granodiorite samples represent magma enriched in biotite and early crystallized plagioclase. At one extreme, sample EL89 contains ~61% accumulated crystals (50% plagioclase and 11% biotite); at the other, sample EL59 contains only 10–15% of accumulated crystals. Intermediate samples represent 60–80% melt. The grey granodiorite samples represent magmas (with >0·4 melt fraction) that were capable of intrusion after crystal accumulation started. Pink leucogranite represents fractionated melt. An analogous pattern can be seen within the parautochthonous plutons; sample EL176 represents an accumulation of plagioclase with 25–30% melt, and sample EL266 a fractionated melt (e.g. Fig. 11).

The principal source of variation in the geochemistry of the granite neosomes is fractional crystallization. Moreover, the effect of fractional crystallization increases with distance ascended (Fig. 13). Nevertheless, some compositional variability still reflects separation of a residuum component, in which the accessory phases were an important constituent. Because the proportion of residuum is least in the farthest-travelled, most-fractionated magmas, and greatest in grey granodiorite samples, the onset of crystallization probably promoted the separation of much of the residuum fraction from the magmas that left the anatectic zone.

DISCUSSION

Field observations from the Opatica show a continuity from palaeosome, patch migmatite and diatexite to parautochthonous granite in the anatectic region, and to allochthonous granite higher in the crust. Similar sequences have been observed in reworked crust elsewhere (Read, 1957; Sederholm, 1967). However, such sequences, and the significance of migmatites within them, have been questioned because of a lack of demonstrated geochemical continuity (White & Chappell, 1990). For example, the sampled diatexite migmatites from St Malo (Brown, 1979), Trois Seigneurs (Wickham, 1987*b*) and Higo (Obata *et al.*, 1994), all plot on the melt side of their respective palaeosomes, which implies addition of melt to the anatectic region and no progression from migmatite to granite. In the Opatica case, the existence of diatexite with residual compositions means that granite formation might have been a closed-system process, with diatexite occupying a critical position in the granite-forming process. The absence of residual diatexite migmatites from other terranes is probably due to incomplete sampling.

Diatexite as magma

The principal, perhaps even definitive, features by which diatexite is recognized in the field are extensive textural modification of the palaeosome which destroys the pre-migmatization structures, and evidence for flow. These features probably reflect the presence of a higher melt fraction (M_F) in diatexite compared with other types of migmatite. Two ways of obtaining the high melt fraction observed in diatexite world-wide have been suggested. Brown (1973) proposed that diatexites are migmatites where the degree of partial melting (F) was high, or that fusion was nearly complete. In such cases, the diatexite is a magma, although not necessarily a granitic one. This origin requires temperatures high enough for F to be large. However, temperatures in the Opatica were probably insufficient for this process to be viable, given the palaeosome bulk compositions. Greenfield *et al.* (1996) described a case where injection of magma from an external source into a partially melted rock increased M_F and generated a diatexite magma. This mechanism does not apply to the Opatica, because there is no chemical or isotopic evidence for an external magma. If neither model applies, then how did the Opatica diatexites form, and were they magmas?

Degree of partial melting

The large volume of anatectic granite in the Opatica, and the very low biotite content of its palaeosome, argues

against biotite dehydration melting as a major source of its granitic rocks. Rather, water-present melting of quartz + plagioclase + K-feldspar seems more probable. Wet melting experiments on granodiorite and tonalite (Wyllie *et al.*, 1976) show that K-feldspar is the first phase to disappear from the palaeosome. Because the anatectic melts and magmas are granitic, and the residual rocks are depleted in K-feldspar, the volume of granite that could have been generated by H_2O-saturated melting was limited by the amount of K-feldspar in the palaeosome, which is between 3 and 13% (average 8%). To produce the granitic mode of a melt generated at 5–7 kbar (Winkler, 1976), the palaeosome could yield between 10 and 48% melt (average 29%). Some biotite may have melted incongruently to leave magnetite and/or titanite in the residuum, because the average biotite/magnetite ratio in the palaeosome is 22, but 17 in the residual rocks. Thus, a maximum of ~20% of palaeosome biotite may have broken down, contributing K-feldspar for a further 3% melt.

The degree of partial melting can be estimated from the incompatible element contents of the palaeosome (C_P) and associated residual diatexite (C_R) using $F = (C_P - C_R)/C_R$ (Sawyer, 1991). Estimates of F range between 0·19 for sample pair EL267–EL267A and 0·48 for pair EL269–EL269A, in agreement with results from the modal mineralogy. Assuming $F = 0{\cdot}5$, the maximum biotite content of the residual diatexite should be twice that of the palaeosome, as Table 1 shows. However, the much higher biotite contents of the schlieren suggest that they did not form by simple melt extraction from a sheared matrix.

By taking an average palaeosome composition and assuming the melt composition to be that of leucosome EL268B, Fig. 9 shows that the melt fraction in the pink diatexite is >0·4, with some samples being essentially all melt (M_F close to unity). If between 10 and 48% melting occurred, then the high M_F of the pink diatexite samples requires that the melt fraction was redistributed. Because the compositional peculiarities of individual palaeosome samples can be traced through residuum, schlieren, pink diatexites and local parautochthonous granite bodies derived from it (Fig. 8), the redistribution of melt was within, and not between, layers. Magma batches were evidently not mixed at the diatexite stage in the Opatica. Hence a third diatexite-forming mechanism is closed-system melt redistribution.

Formation of granitic magma

Noting that crustal melting and heterogeneous deformation are generally synchronous, Sawyer (1994) proposed that the melt fraction would be squeezed out of the deforming matrix as it formed, and collect to form magma in low-pressure sites. The small granitic veins (migmatite leucosomes) in rocks that preserve the earliest stage of migmatization are evidence of this deformation-assisted melt segregation process in the Opatica. This concept of melt–residuum segregation was developed for the leucosomes in metatexite migmatites and is not directly applicable to the formation of large volumes of granitic magma. This is because the magma compositions produced are generally too leucocratic (Clemens & Mawer, 1992; Whitney & Irving, 1994) to be the parental magma of most granites (Sawyer, 1996).

In the Opatica the melt fraction was not removed as it formed in every case. Some grey diatexite samples have bulk compositions similar to the palaeosome, but also contain evidence for bulk flow, which implies the presence of melt. This suggests that the melt generation rate exceeded the melt segregation rate (Sawyer, 1994). This in turn implies that rapid melt generation occurred as a result, perhaps, of underplating, rapid uplift or an influx of water. Residual diatexite samples without K-feldspar represent domains where all the melt was removed from grey diatexite, whereas those that have minor amounts of K-feldspar along grain boundaries retained a small melt fraction. However, melt removal was still a filter-pressing type of process and it should have produced magmas with very little residuum. Because the partially melted layers were sandwiched between infertile, more competent grey gneiss layers, the melt fraction was confined to move within the partially melted layer during deformation rather than between layers. As melt began to move and accumulate, the local permeability increased because of a rise in melt fraction. This both aided and focused melt migration. Stevenson (1989) has shown that melt will move to sites where it has already accumulated. Thus, the redistribution of the melt fraction created melt-enriched pink diatexite at site of melt accumulation. A consequence of competent wall rocks, shearing and melt flow is that the magma fluid pressure will rise. This can cause fracturing, but, more probably, cause the disaggregation of the host by inflating the melt film along grain boundaries. This process reincorporates residual material back into the melt, principally as disaggregated grains, but also as xenoliths. This contaminated diatexite magma was the source for the parautochthonous plutons in the migmatite zones and the dykes, sills and plutons at higher crustal levels.

Once the melt fraction in the pink diatexites became large enough for magma flow, three other processes which can separate residuum from melt could begin. First, because the velocity distribution of residual particles might not be uniform when magma flow began, some particle interactions will occur and build up aggregates of residuum grains. Second, particles and aggregates in the magma may have rotated during flow. If some were close enough to each other to interact, they could have

piled against one another, to form imbricated aggregates of oriented grains (Blumenfeld & Bouchez, 1988), such as those observed in the schlieren (Fig. 3d). Finally, if individual particles, or aggregates of residuum grains, had large aspect ratios, then flow would have generated a dispersive pressure (Bagnold, 1954, 1956), known as the Bagnold Effect, which would have concentrated and aligned the solid particles into layers or trains in the flowing magma, thus forming the semi-continuous flow bands of schlieren. Such processes could have both progressively formed the schlieren and reduced the residuum component in the granite magma.

The final stage of melt segregation occurred as the migmatite region cooled. Small amounts of remaining (residual) melt trapped in nearly solidified diatexite were expelled during minor shearing. This formed the coarse-grained and highly fractionated leucocratic veins (e.g. sample EL179) which post-date the flow banding in diatexite.

CONCLUSIONS

The morphological continuity observed in the field across the palaeosome to granite transition is mirrored by progressive changes in texture, mineralogy and geochemistry. This suggests that anatexis and crustal reworking in the Opatica subprovince occurred as an essentially closed-system process.

The creation of diatexite migmatite is the key step in the palaeosome to granite transition, because granitic magma originates from such rocks. The principal processes involved are redistribution and contamination of the melt fraction with some of the residuum it passes through. Large volumes of residual material are produced from diatexites as they lose their melt fraction. However, diatexite magmas are created in parts of diatexites where this melt fraction accumulates. Diatexite magma is parental to the parautochthonous and allochthonous granites higher in the crust.

During the migration of diatexite magma out of its source layer to higher levels within the anatectic region, its composition is modified by the removal of residuum minerals into schlieren and, to a lesser degree, by fractional crystallization. However, once magma ascends out of the anatectic zone and traverses cooler crust it begins to crystallize. At these crustal levels, fractional crystallization becomes the dominant factor in controlling magma compositions.

ACKNOWLEDGEMENTS

I would like to thank Don Baker, Sarah-Jane Barnes, Mike Brown, Bill Collins, Isabel Milord, Tracy Rushmer and Gary Solar for their critical comments and encouragement during this project. Comments provided by the Journal reviewers, John Ashworth, Calvin Barnes and Alberto Patiño-Douce, and editor Sorena Sorensen are greatly appreciated. This study was funded by NSERC collaborative project grant 183274 and individual operating grant 1928.

REFERENCES

Bagnold, R. A. (1954). Experiments on a gravity-free dispersion of large solid spheres in a Newtonian fluid under shear. *Proceedings of the Royal Society of London, Series A* **A249,** 49–53.

Bagnold, R. A. (1956). The flow of cohesionless grains in a fluid. *Philosophical Transactions of the Royal Society of London, Series A* **249,** 235–297.

Bea, F. (1991). Geochemical modeling of low melt-fraction anatexis in a peraluminous system: the Pena Negra Complex (central Spain). *Geochimica et Cosmochimica Acta* **55,** 1859–1874.

Bédard, L. P. & Barnes, S.-J. (1990). Instrumental neutron activation analysis by collecting only one spectrum: results for international geochemical reference samples. *Geostandards Newsletter* **14,** 479–484.

Bédard, L. P. & Ludden, J. N. (1997). Nd-isotope evolution of Archaean plutonic rocks in the southeastern Superior Province. *Canadian Journal of Earth Sciences* **34,** 286–298.

Bellefleur, G., Calvert, A. J. & Chouteau, M. C. (1998). Crustal geometry of the Abitibi subprovince in light of 3D seismic reflector orientations. *Canadian Journal of Earth Sciences*, in press.

Benn, K., Sawyer, E. W. & Bouchez, J.-L. (1992). Orogen parallel and transverse shearing in the Opatica belt, Quebec: implications for the structure of the Abitibi Subprovince. *Canadian Journal of Earth Sciences* **29,** 2429–2444.

Blumenfeld, P. & Bouchez, J.-L. (1988). Shear criteria in granite and migmatite deformed in the magmatic and solid states. *Journal of Structural Geology* **10,** 361–372.

Brown, M. (1973). Definition of Metatexis, Diatexis and Migmatite. *Proceedings of the Geologists' Association* **84,** 371–382.

Brown, M. (1979). The petrogenesis of the St Malo Migmatite Belt, Armorican Massif, France, with particular reference to the diatexites. *Neues Jahrbuch für Mineralogie, Abhandlungen* **135,** 48–74.

Brown, M., Averkin, Y. A., McLellan, E. L. & Sawyer, E. W. (1995). Melt segregation in migmatites. *Journal of Geophysical Research* **100,** 15655–15679.

Calvert, A. J., Sawyer, E. W., Davis, W. J. & Ludden, J. N. (1995). Archaean subduction inferred from seismic images of a mantle suture in the Superior Province. *Nature* **375,** 670–674.

Chappell, B. W. (1996). Compositional variation within granite suites of the Lachlan Fold Belt: its causes and implications for the physical state of granite magma. *Transactions of the Royal Society of Edinburgh: Earth Sciences* **88,** 159–170.

Clemens, J. D. & Mawer, C. K. (1992). Granitic magma transport by fracture propagation. *Tectonophysics* **204,** 339–360.

Davis, W. J., Machado, N., Gariepy, C., Sawyer, E. W. & Benn, K. (1995). U–Pb geochronology of the Opatica tonalite–gneiss belt and its relationship to the Abitibi greenstone belt, Superior Province, Quebec. *Canadian Journal of Earth Sciences* **32,** 113–127.

Fyfe, W. S. (1973). The granulite facies, partial melting and the Archaean crust. *Philosophical Transactions of the Royal Society of London, Series A* **273,** 457–461.

Greenfield, J. E., Clarke, G. L., Bland, M. & Clarke, D. J. (1996). In-situ migmatite and hybrid diatexite at Mt Stafford, central Australia. *Journal of Metamorphic Geology* **14,** 413–426.

Irvine, T. N. & Barragar, W. R. A. (1971). A guide to the chemical classification of the common rocks. *Canadian Journal of Earth Sciences* **8,** 523–548.

Kohn, M. J. & Spear, F. S. (1990). Two new geobarometers for garnet amphibolites, with application to southeastern Vermont. *American Mineralogist* **75,** 89–96.

Lacroix, S. & Sawyer, E. W. (1995). An Archaean fold–thrust belt in the northwestern Abitibi greenstone belt: structural and seismic evidence. *Canadian Journal of Earth Sciences* **32,** 97–112.

Lambert, I. B. & Heier, K. S. (1968). Geochemical investigations of deep-seated rocks in the Australian Shield. *Lithos* **1,** 30–53.

Le Fort, P. (1981). Manaslu leucogranite: a collisional signature of the Himalaya. A model for its genesis and emplacement. *Journal of Geophysical Research* **86,** 10545–10568.

Miller, C. F., Watson, E. B. & Harrison, T. M. (1988). Perspectives on the source, segregation and transport of granitoid magmas. *Transactions of the Royal Society of Edinburgh: Earth Sciences* **79,** 135–156.

Miller, C. F., Hanchar, J. M., Wooden, J. L., Bennet, V. C., Harrison, T. M., Wark, D. A. & Foster, D. A. (1992). Source region of a granite batholith: evidence from lower crustal xenoliths and inherited accessory minerals. *Transactions of the Royal Society of Edinburgh: Earth Sciences* **83,** 49–62.

Montel, J. M., Didier, J. & Pichavant, M. (1991). Origin of surmicaceous enclaves in intrusive granites. In: Didier, J. & Barbarin, B. (eds) *Enclaves and Granite Petrology*. Amsterdam: Elsevier, pp. 509–528.

Obata, M., Yoshimura, Y., Nagakawa, K., Odawara, S. & Osanai, Y. (1994). Crustal anatexis and melt migrations in the Higo metamorphic terrane, west–central Kyushu, Kumamoto, Japan. *Lithos* **32,** 135–147.

Peacock, M. A. (1931). Classification of igneous rock series. *Journal of Geology* **39,** 54–67.

Read, H. H. (1957). *The Granite Controversy*. London: Murby.

Saunders, A. D., Tarney, J. & Weaver, S. D. (1980). Transverse geochemical variations across the Antarctic Peninsula: implications for the genesis of calc-alkaline magmas. *Earth and Planetary Science Letters* **46,** 344–360.

Sawyer, E. W. (1991). Disequilibrium melting and the rate of melt–residuum separation during migmatisation of mafic rocks from the Grenville Front, Quebec. *Journal of Petrology* **32,** 701–738.

Sawyer, E. W. (1994). Melt segregation in the continental crust. *Geology* **22,** 1019–1022.

Sawyer, E. W. (1996). Melt segregation and magma flow in migmatites: implications for the generation of granite magmas. *Transactions of the Royal Society of Edinburgh: Earth Sciences* **87,** 85–94.

Sawyer, E. W. & Barnes, S.-J. (1988). Temporal and compositional differences between subsolidus and anatectic migmatite leucosomes from the Quetico metasedimentary belt, Canada. *Journal of Metamorphic Geology* **6,** 437–450.

Sawyer, E. W. & Benn, K. (1993). Structure of the high-grade Opatica Belt and adjacent low-grade Abitibi Subprovince, Canada: an Archaean mountain front. *Journal of Structural Geology* **15,** 1443–1458.

Schmidt, M. W. (1992). Amphibole composition in tonalite as a function of pressure: an experimental calibration of the Al-in-hornblende barometer. *Contributions to Mineralogy and Petrology* **110,** 304–310.

Schumacher, R., Schenk, V., Raase, P. & Vitanage, P. W. (1989). Granulite facies metamorphism of metabasic and intermediate rocks in the Highland Series of Sri Lanka. In: Ashworth, J. R. & Brown, M. (eds) *High-Temperature Metamorphism and Crustal Anatexis*. London: Unwin Hyman, pp. 235–271.

Sederholm, J. J. (1967). *Selected Works: Granites and Migmatites*. Edinburgh: Oliver & Boyd.

Spear, F. D. (1981). An experimental study of hornblende stability and compositional variability in amphibolite. *American Journal of Science* **281,** 697–734.

Stevenson, D. J. (1989). Spontaneous small scale melt segregation in partial melts undergoing deformation. *Geophysical Research Letters* **66,** 1067–1070.

Taylor, S. R. & Gorton, M. P. G. (1977). Geochemical application of spark source mass spectrometry—III. Element sensitivity, precision and accuracy. *Geochimica et Cosmochimica Acta* **41,** 1375–1380.

Taylor, S. R. & McLennan, S. M. (1985). *The Continental Crust: its Composition and Evolution*. Oxford: Blackwell.

Tindle, A. G., McGarvie, D. E. & Webb, P. C. (1988). The role of hybridization and crystal fractionation in the evolution of the Cairnsmore of Carphairn Intrusion, Southern Uplands of Scotland. *Journal of the Geological Society, London* **145,** 11–21.

Watson, E. B. & Harrison, T. M. (1983). Zircon saturation revisited: temperature and composition effects in a variety of crustal magma types. *Earth and Planetary Science Letters* **64,** 295–304.

White, A. J. R. & Chappell, B. W. (1990). Per migma ad magma downunder. *Geological Journal* **25,** 221–225.

Whitney, D. L. & Irving, A. J. (1994). Origin of K-poor leucosomes in a metasedimentary migmatite complex by ultrametamorphism, synmetamorphic magmatism and subsolidus processes. *Lithos* **32,** 173–192.

Wickham, S. M. (1987*a*). The segregation and emplacement of granitic melts. *Journal of the Geological Society, London* **144,** 281–297.

Wickham, S. M. (1987*b*). Crustal anatexis and granite petrogenesis during low-pressure regional metamorphism: the Trois Seigneurs Massif, Pyrenees, France. *Journal of Petrology* **28,** 127–169.

Winkler, H. G. F. (1976). *Petrogenesis of Metamorphic Rocks*. New York: Springer Verlag.

Wyllie, P. J., Huang, W.-L., Stern, C. & Maaloe, S. (1976). Granitic magmas: possible and impossible sources, water contents, and crystallization sequences. *Canadian Journal of Earth Sciences* **13,** 1007–1019.